

Chapter 42

Synthesis of Co-ordination Energetic Graphene Oxide and Thermal Decomposition for the Combustion of Ammonium Perchlorate



Haibo Ke, Zhe Zhang, Wang Wang, Yu Cheng, Qiangqiang Lu, Dongqi Liu, Lei Xiao, Fengqi Zhao, Wei Jiang, and Gazi Hao

Abstract In this study, a new co-ordination energetic graphene oxide (CEGO) based on Cu^{2+} as the co-ordination centre was synthesised using 4-amino-1,2,4-triazole as the energetic ligand. X-ray diffractometry, scanning electron microscopy, Fourier transform infrared spectroscopy and X-ray photoelectron spectroscopy results showed that CEGO was successfully synthesised. Then, the catalytic effect of CEGO on the thermal decomposition of ammonium perchlorate (AP) was investigated using differential scanning calorimetric techniques and thermogravimetric analysis. The results revealed that the decomposition peak temperature and Gibbs free energy of the CEGO/AP composite decreased by $88.4\text{ }^{\circ}\text{C}$ and 13.7 kJ/mol compared with pure AP, respectively. At this time, compared with pure AP (132.9 J/g) and other AP composites, the heat release of the CEGO/AP composite increased to 1580.6 J/g , which was the highest. Overall, as an energetic combustion catalyst, CEGO has a significant catalytic effect on AP and can be incorporated into AP-based propellants.

H. Ke · W. Wang · Q. Lu · D. Liu · L. Xiao · W. Jiang · G. Hao (✉)

National Special Superfine Powder Engineering Research Center of China, School of Chemistry and Chemical Engineering, Nanjing University of Science and Technology, Nanjing 210094, China

e-mail: hgznjust1989@163.com

D. Liu

e-mail: ldqnjust1997@163.com

L. Xiao

e-mail: 15005161138@163.com

W. Jiang

e-mail: superfine_jw@126.com

Z. Zhang · Y. Cheng

Shanghai Space Propulsion Technology Research Institute, Huzhou 313000, China

e-mail: zzfarfromok@163.com

F. Zhao

Xi'an Modern Chemistry Research Institute, Xi'an 710065, China

e-mail: zhaofqi@163.com

© China Ordnance Society 2022

A. Gany and X. Fu (eds.), 2021 *International Conference on Development and Application of Carbon Nanomaterials in Energetic Materials*, Springer Proceedings in Physics 276, https://doi.org/10.1007/978-981-19-1774-5_42

42.1 Introduction

Ammonium perchlorate (AP), a widely used oxidant, plays a crucial role in solid propellant systems. To some extent, the combustion performance of AP affects the energy output of the overall propellant system; thus, considerable efforts have been made to improve the combustion performance of AP [1–3]. Moreover, it was reported that adding a combustion catalyst to an AP system can significantly accelerate the thermal decomposition process of the AP, thereby improving the overall performance of the AP-based propellant such as ballistic performance, combustion performance and energy level [4]. Therefore, it is pertinent to incorporate combustion catalysts into AP.

Initially, common materials used for combustion catalysts include nano-metals and their oxides (such as Fe_2O_3), composite metal complexes (such as CuCr_2O_4) and composite combustion catalysts [such as CuO /graphene oxide (GO)] [5–9]. Metal oxides are traditional combustion catalysts and have good performance. For example, Zhang et al. [10] controlled the compounding time to study the best catalytic effect of nano- CuCr_2O_4 on an ultrafine AP. When the milling time was in the range of 6–12 h, nano- CuCr_2O_4 was most evenly dispersed on the ultrafine AP. At this time, the decomposition temperature and Gibbs free energy of the nano- CuCr_2O_4 /ultrafine AP composite were the lowest, which decreased by 78.1 °C and 25.16 kJ/mol, respectively. In addition, Alizadeh-Gheshlaghi et al. [11] synthesised CuCo_2O_4 via the sol–gel method, which could advance the peak temperature of AP decomposition from 443.6 to 340.8 °C and had good catalytic activity for AP. However, the catalytic performance of these inert combustion catalysts encounters bottlenecks in the catalytic process, which cannot meet the future development requirements of high-energy AP-based propellants.

With the development of science and technology, GO, as a two-dimensional carbon material, has attracted extensive research attention due to its large specific surface area, excellent electrical and thermal conductivity as well as unique band structure [12–15]. It was found that when nano-metal oxides were loaded on GO sheets because GO could accelerate electron transfer during the decomposition of AP, synergistic catalysis with nano-metal oxides could significantly improve the catalytic thermal decomposition rate of AP. For example, Li et al. [16] successfully loaded Mn_3O_4 onto graphene (GR) sheets via the solvothermal method to form a Mn_3O_4 /GR nano-composite. The results showed that the nano-composite had a good catalytic effect on AP; it could reduce the high-temperature decomposition peak temperature of AP by 141.9 °C. Zhu et al. [17] used the in situ deposition method to load CuO nano-particles onto GO sheets to form a CuO /GO nano-composite. It was found that the high-temperature decomposition peak temperature of AP advanced from 414 to 315 °C with the addition of 2-wt% CuO /GO nano-composites, and the catalytic effect was better than that of a single-component CuO (334 °C). Although the GO composite catalyst significantly increases the thermal decomposition rate of AP, the catalyst itself is not an energetic component; therefore, energy is wasted in the process of catalysing AP and propellants.

Recently, the energisation of GO has become a hot topic because there are numerous oxygen-containing groups on the surface of GO sheets, such as $-\text{COOH}$, $-\text{OH}$ and $\text{C}-\text{O}-\text{C}$, which broadens the idea of functional modification of GO, such as modifying energetic components on the surface of GO through acylation or esterification reactions [18–20]. Thus, the energy level and catalytic activity can be improved. For example, Zhang et al. [21] prepared a monolayer nanoscale GO (NGO) with the nitro group via the nitrification of GO with mixed sulphur and nitrate acid. It was found that when 10-wt% NGO was added, the high-temperature decomposition peak temperature advanced by 106 °C and the apparent decomposition heat of AP increased from 875 to 3236 J/g, indicating that NGO had a significant catalytic effect on AP and considerably improved the apparent decomposition heat of AP. Therefore, GO can be energised and used as an energetic combustion catalyst for an AP-based propellant system, which solves the problem of energy reduction due to the introduction of an inert combustion catalyst to a certain extent.

However, the covalent modification of GO still has some drawbacks. Because the activity of oxygen-containing groups on the surface of GO is not high, organic reagents are often added to activate the functional modification of GO, which makes the experimental process and subsequent separation and purification more complicated [22–24]. By contrast, the co-ordination modification on the GO matrix has become a popular idea [25]. For example, Cohen et al. [26] synthesised two energetic complexes based on GO using 5,5'-azo-1,2,3,4-tetrazole and 4,4'-azo-1,2,4-triazole as ligands and Cu^{2+} as the co-ordination centre. The energetic complexes had low sensitivity, high thermal stability and the same detonation performance as hexahydro-1,3,5-trinitro-1,3,5-triazine (RDX). Moreover, Zhang et al. [27] prepared several novel GO-based bis-tetrazole energetic co-ordination polymers (ECPs) via the solvothermal method. These ECPs as energetic catalysts had a significant catalytic effect on the thermal decomposition of AP and RDX. The heat releases of AP and RDX catalysed by GR-templated bis-tetrazoles were 2757.0 and 2898.0 J/g, respectively, which improved more than 50% compared with pure AP and RDX. The endothermic peak of AP corresponding to the crystal transformation also reduced to 23.2 kJ/mol. The successful preparation of such energetic co-ordination compounds confirmed the feasibility of the idea of co-ordination modification of GO.

In this study, a novel Cu^{2+} co-ordination energetic GO (CEGO), which comprised GO, 4-amino-1,2,4-triazole (ATA) and Cu^{2+} , was synthesised through co-ordination bonds of which ATA is the energetic ligand. As a high azole compound, ATA has excellent energy performance and high enthalpy of formation and is eco-friendly with low impact sensitivity [28–30]. Moreover, nitrogen atoms in its ring have lone pair electrons and abundant co-ordination sites, which are easy to co-ordinate with transition metals. In addition, GO has excellent electron transport performance. Cu^{2+} with good catalytic activity is used as the co-ordination centre to bond the former two substances through co-ordination bonds to achieve a synergistic catalytic effect. Further, the structure of CEGO is characterised in detail, and its catalytic performance for AP is studied as a combustion catalyst.

42.2 Experimental

All reagents were of analytical grade, except AP, and they were directly used without further purification. AP was of industrial grade and was purchased from Dalian Perchloric Acid Ammonium Factory. GO was purchased from Suzhou Tanfeng Graphene Technology Co., Ltd. 4-amino-1,2,4-triazol, CuO and $\text{Cu}(\text{NO}_3)_2$ were purchased from Shanghai Macklin Biochemical Co., Ltd. Ethyl acetate was purchased from Nanjing Chemical Reagent Co., Ltd.

42.2.1 Synthesis of CEGO

In this subsection, we present the details of the synthesis of CEGO. First, GO was added to deionised water and ultrasonically dispersed at 20 °C for 30 min to obtain a dispersed GO solution (50 mL, 1.0 mg/mL). Then, 282 mg (1.5 mmol) $\text{Cu}(\text{NO}_3)_2$ was weighed and dissolved in 20 mL deionised water. After ultrasonic dispersion for 30 min, it was slowly added to GO dispersion, heated and stirred at 60 °C for 12 h to obtain a black–green mixed solution. Afterwards, it was ultrasonically separated into the ATA solution (10 mL, 16.8 mg/mL), added to the mixed system, stirred and heated at 60 °C for 12 h. Finally, it was centrifuged for washing and vacuum freeze-dried for 24 h to obtain CEGO.

42.2.2 Synthesis of CEGO/AP and Other AP Composites

The CEGO/AP composite was synthesised by simple mechanical grinding methods. The details are as follows. First, CEGO and pure AP were mixed at a mass ratio of 5:95 to obtain a mixture of 40 mg and placed in a mortar, and ethyl acetate (1 mL) was added. To avoid changing the particle size of the mixture as much as possible, the grinding strength was controlled, which meant gently grinding for 30 min until everything was properly mixed. Finally, the mixture was dried for 20 min in a 60 °C oven. A CEGO/AP composite with 5-wt% CEGO was obtained after complete drying.

Further, other AP composites were synthesised with the same mass ratio; the synthesised composites include ATA/AP, CuO/AP and GO/AP.

42.2.3 Measurements

Powder X-ray diffractometry (XRD) was performed with a Rigaku smartlab9 instrument at voltage and current of 40 kV and 150 mA, respectively. Fourier transform

infrared (FT-IR) spectroscopy of the samples was performed (Nicolet iS5) in the range of 400–4000 cm^{-1} . The morphology of ATA was examined using a stereoscopic microscope (Leica M165), and those of GO and CEGO were examined using a high-resolution thermal field scanning electron microscope (Quanta 400 FEG) equipped with an energy dispersion X-ray spectrometer (EDS); corresponding chemical compositions were determined using the EDS. X-ray photoelectron spectroscopy (XPS) measurements were performed using an ESCALAB 250Xi spectrometer equipped with a pass energy of 30 eV with a power of 100 W (10 kV and 10 mA) and a monochromatised Al-K α X-ray source. In addition, scanning electron microscopy (SEM) was performed.

The thermal analysis experiment was performed using METTLER TOLEDO TGA/DSC3+; the N_2 flow rate was 50 ml/min, the selected heating rate was 5, 10, 15 and 20 $^\circ\text{C}/\text{min}$, and the system was heated from 35 to 520 $^\circ\text{C}$. The kinetic parameters for the exothermic decomposition of pure AP and AP composites were obtained using the Kissinger method [31].

42.3 Results and Discussion

In this study, CEGO was synthesised in two steps. First, Cu^{2+} was connected by co-ordination bonds to oxygen atoms in the GO sheets, which were mainly provided by oxygen-containing groups ($-\text{COOH}$, $-\text{OH}$). Further, nitrogen atoms in ATA co-ordinated with Cu^{2+} to yield CEGO. The corresponding synthesis process of CEGO is illustrated in Fig. 42.1.

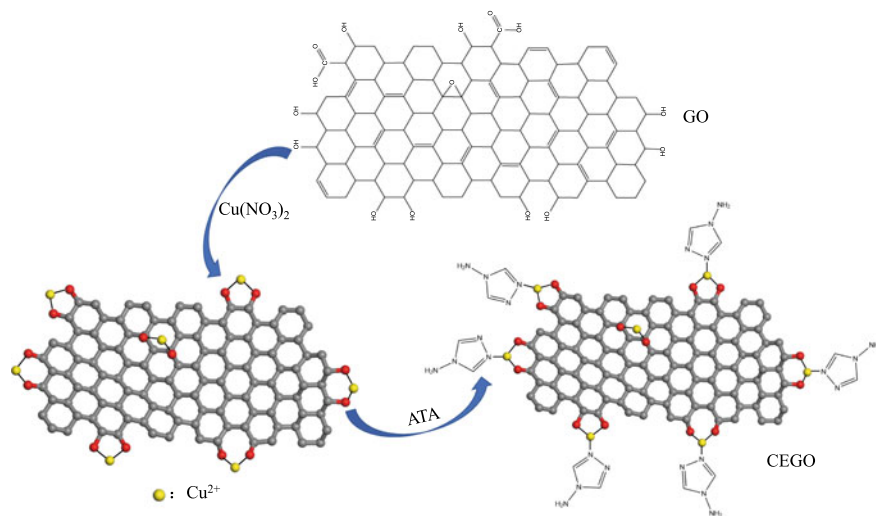


Fig. 42.1 Synthesis process of co-ordination energetic graphene oxide (CEGO)

42.3.1 XRD and FT-IR Analyses

The structural information of ATA, GO and CEGO was analysed using XRD and FT-IR.

Figure 42.2 depicts the XRD patterns of ATA, GO and CEGO. The peak with the highest GO diffraction intensity corresponds to $2\theta = 8.9^\circ$, which is quite similar to CEGO ($2\theta = 10.0^\circ$), indicating that the co-ordination modification process slightly affected the structure of GO. Moreover, the XRD pattern of CEGO displays a broad diffraction peak near $2\theta = 24.6^\circ$, possibly attributed to the co-ordination of ATA on CEGO sheets, which is consistent with the regional concentration of ATA diffraction peaks. However, the characteristic peaks of Cu^{2+} were not found in the XRD spectrum of CEGO, which was probably because the content of Cu^{2+} was too small to reach the detection range.

To verify the successful functionalisation of GO, FT-IR spectroscopy of GO and CEGO were performed (Fig. 42.3). Compared with GO, the characteristic peaks of

Fig. 42.2 XRD patterns of 4-amino-1,2,4-triazole (ATA), graphene oxide (GO) and CEGO

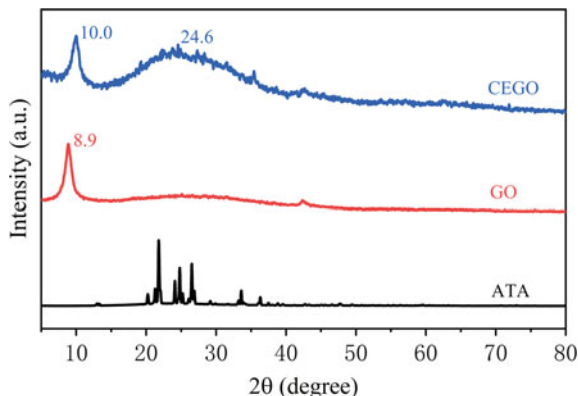
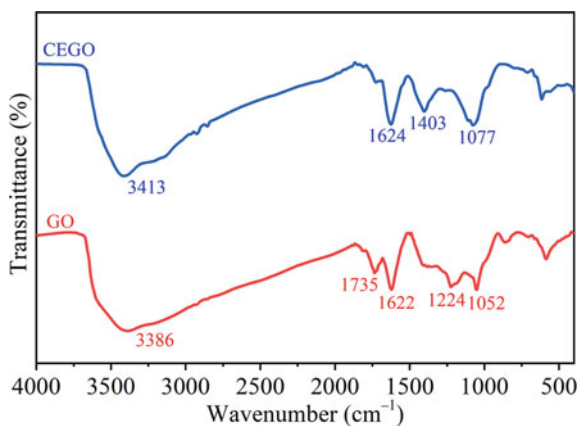


Fig. 42.3 FT-IR spectra of GO and CEGO



CEGO at 1735 and 1224 cm^{-1} , corresponding to the characteristic peaks of $\text{C}=\text{O}$ and $\text{C}-\text{OH}$, respectively, disappeared. The carbonyl group ($\text{C}=\text{O}$) belongs to the carboxyl group in the GO surface functional group, and $\text{C}-\text{OH}$ belongs to the hydroxyl group. Cu^{2+} formed co-ordination bonds with hydroxyl and carboxyl groups, which led to the disappearance of the two characteristic peaks. The characteristic peak of CEGO at 1624 and 1077 cm^{-1} are attributed to the stretching vibration peak of the $\text{C}=\text{C}$ and $\text{C}-\text{O}$ bonds, respectively. In addition, CEGO had a new characteristic peak at 1403 cm^{-1} , corresponding to the $-\text{NH}$ bond, which came from ATA. Finally, the FT-IR results showed that Cu^{2+} and ATA were connected to GO through co-ordination bonds, and CEGO was successfully synthesised.

42.3.2 SEM and EDS Analyses

The morphology of ATA measured using a stereoscopic microscope is depicted in Fig. 4a. As shown in Fig. 4a, ATA was white transparent crystal particles. Owing to its high hygroscopicity, the crystal particles quickly bonded into clusters in the air. Figure 4b–h shows SEM images and EDS surface elemental analyses of GO and CEGO. The stacked GO sheets had several wrinkles (Fig. 4b), which was mainly due to the varying degrees of oxidation on the surface of the sheets. The CEGO sheets (Fig. 4c) exhibited a rough bulky surface, probably due to the complexation with Cu^{2+} and co-ordination with the ligands. CEGO was tested using EDS to obtain the distribution of the C, N, O and Cu elements (Fig. 4d–h). Among them, the O element belonged to the GO surface oxidation functional group. Further, the EDS surface elemental analyses confirmed the presence of Cu and N atoms, indicating that the GO bonded with Cu, which in turn co-ordinated with the ATA ligands.

42.3.3 XPS Analysis

To further verify the chemical-binding relationship between GO and Cu^{2+} and the energetic ligand (ATA), XPS was employed. In the survey spectra (Fig. 5a), compared with GO, there is an obvious N 1 s peak, and new peaks of Cu $2p_{1/2}$ and Cu $2p_{3/2}$ appeared in the CEGO spectrum. In Fig. 5b, the peak-fitting spectra of C 1 s of GO clearly indicate a considerable degree of oxidation, showing different oxygen-containing functional groups. CEGO showed new peaks in C 1 s curves (Fig. 5c), attributable to the formation of co-ordination bonds between Cu^{2+} and oxygen-containing groups on the GO sheets; $\text{C}-\text{O}-\text{Cu}$ bonds (287.5 eV) were obtained, and the C 1 s peak at 285.8 eV ($\text{C}-\text{N}$) originated from further co-ordination of ATA with Cu^{2+} . The corresponding co-ordination effect was more obvious in the peak-fitting spectra of N 1 s of CEGO (Fig. 5d), including the N 1 s peaks at 399.9 eV ($=\text{N}-$) and 400.7 eV (NH , $-\text{N}-\text{N}-$). In addition, the positively charged N^+ at 402.1 eV was formed due to the successful co-ordination with the Cu^{2+} , and a trace amount

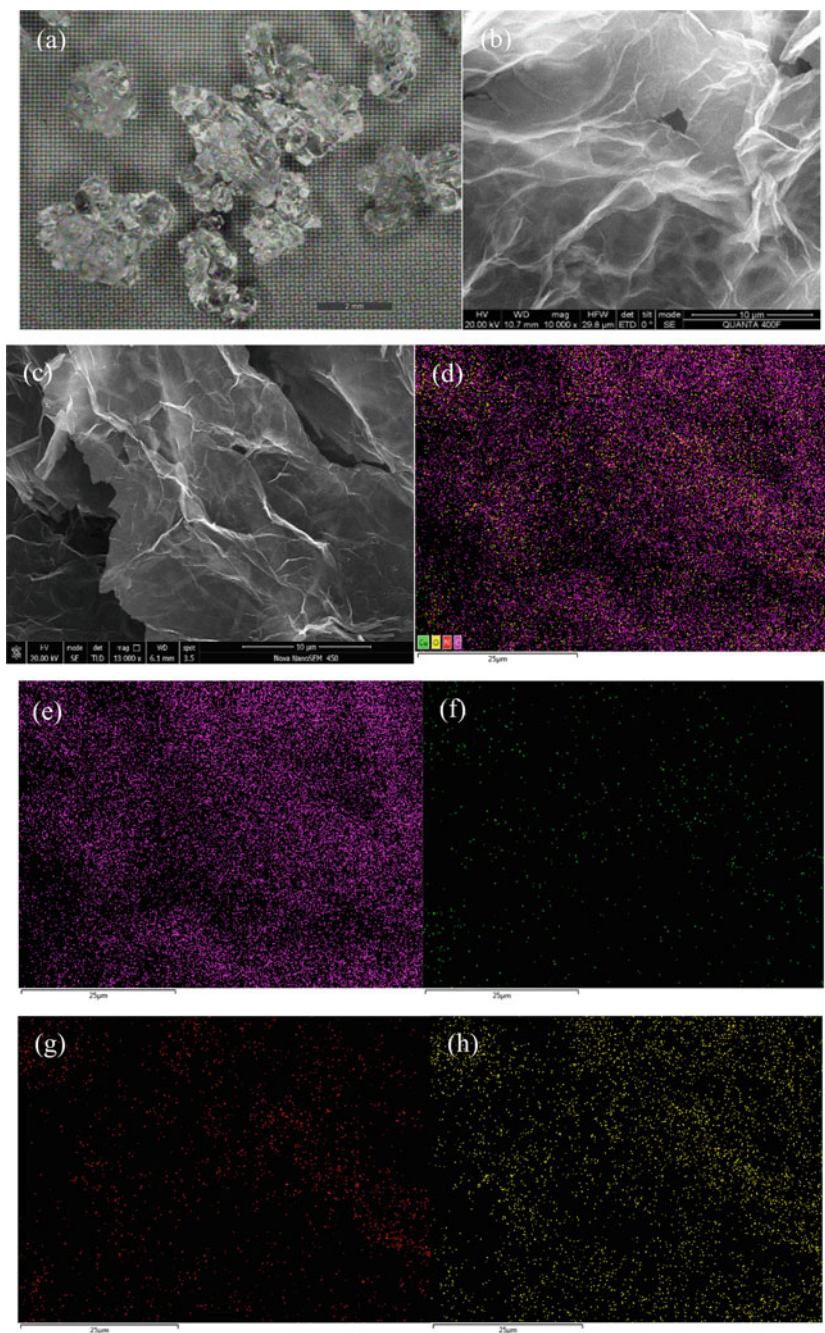


Fig. 42.4 The morphology of **a** ATA; SEM of **b** GO and **c** CEGO; **d–h** EDS of CEGO

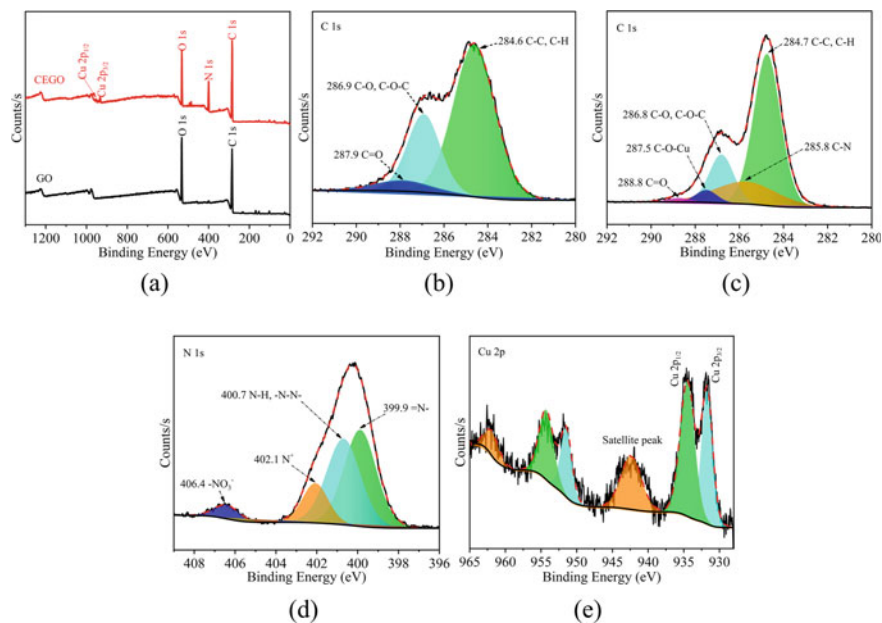


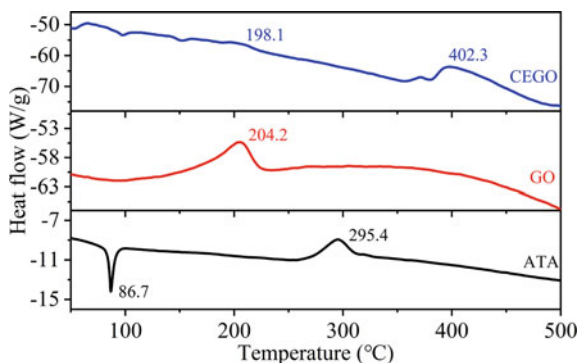
Fig. 42.5 XPS spectra of **a** the survey spectra of GO and CEGO; **b** the peak-fitting spectra of C 1 s of GO; **c–e** the peak-fitting spectra of C 1 s, N 1 s and Cu 2p of CEGO

of NO_3^- was observed (406.4 eV). The XPS of Cu 2p (Fig. 5e) was divided into two peaks of 731.7 and 734.5 eV, belonging to the Cu $2p_{1/2}$ and Cu $2p_{3/2}$ spin-orbit peaks of Cu^{2+} , respectively, which could be assigned to the corresponding Cu–O and Cu–N bonds, respectively.

42.3.4 Catalytic Performance of CEGO/AP and Other AP Composites

Figure 42.6 shows the DSC curves of ATA, GO and CEGO at a heating rate of $10\text{ }^\circ\text{C}/\text{min}$. The CEGO was reported to mainly decompose with a peak temperature of $402.3\text{ }^\circ\text{C}$, accompanied by a small amount of decomposition at $198.1\text{ }^\circ\text{C}$, which was close to the temperature decomposition peak of GO ($204.2\text{ }^\circ\text{C}$), corresponding to the decomposition and shedding of oxygen-containing groups on the GO sheets. In addition, there was an endothermic peak of the energetic complex (ATA) at $86.7\text{ }^\circ\text{C}$, which was inferred to the crystal transformation takes place at this stage. With the increase of temperature, the ATA decomposed and exothermed, and the corresponding peak temperature was $295.4\text{ }^\circ\text{C}$ at this time, which was $106.9\text{ }^\circ\text{C}$ lower than the temperature decomposition peak of CEGO, indicating that the thermal stability of CEGO was significantly increased after the formation of ATA and GO

Fig. 42.6 DSC curves of ATA, GO and CEGO at a heating rate of 10 °C/min



complex. Moreover, compared with GO (988.6 J/g), CEGO had a fairly high heat release (3167.2 J/g).

Table 42.1 shows the thermal decomposition performance data of pure AP and AP composites. The differential scanning calorimetric (DSC) and thermogravimetric (TG) curves of pure AP and AP composites at a heating rate of 10 °C/min are depicted in Fig. 42.7. From Fig. 7a, compared with pure AP's two distinct periods of weightlessness, AP composites tended to fuse during the two weightlessness stages; the CEGO/AP showed only one weightlessness stage. The corresponding effect could also be seen in the DSC curve (Fig. 7b), the low-temperature decomposition peak of CEGO/AP disappeared, the high-temperature decomposition peak temperature, T_H , advanced from 419.2 to 330.8 °C and the heat release was the highest (1580.6 J/g), whereas the heat release for pure AP was only 132.9 J/g. Moreover, from the TG curves and Table 42.1, the initial decomposition temperature of CuO/AP was significantly earlier than that of other AP composites, the low- and high-temperature decomposition peak temperature, T_L and T_H , respectively, of the corresponding DSC curve advanced by 31.1 °C and 83.9 °C respectively, but the heat release (1101.8 J/g) was lower than that of CEGO/AP. By contrast, the catalytic effect of GO on AP was not obvious, the T_H moved forward by only 21.7 °C (Fig. 7b), which might be because the oxygen-containing groups on GO reduced the conductivity between the lamellar and

Table 42.1 Thermal decomposition performance data of pure AP and AP composites

| Sample | T_e (°C) | T_c (°C) | T_m (°C) | T_L (°C) | T_H (°C) | Q (J/g) |
|---------|------------|------------|------------|------------|------------|-----------|
| AP | 276.8 | 417.6 | 406.6 | 297.9 | 419.2 | 132.9 |
| CuO/AP | 255.9 | 343.4 | 333.4 | 266.8 | 335.3 | 1101.8 |
| ATA/AP | 272.4 | 380.8 | 319.7 | – | 320.9 | 1042.0 |
| GO/AP | 264.5 | 396.8 | 389.1 | 289.6 | 397.5 | 352.1 |
| CEGO/AP | 258.1 | 339.8 | 330.8 | – | 330.8 | 1580.6 |

Note T_e is the initial decomposition temperature; T_c is the terminal decomposition temperature; T_m is the maximum weight loss temperature; T_L is the low-temperature decomposition peak temperature; T_H is the high-temperature decomposition peak temperature; Q is the heat release

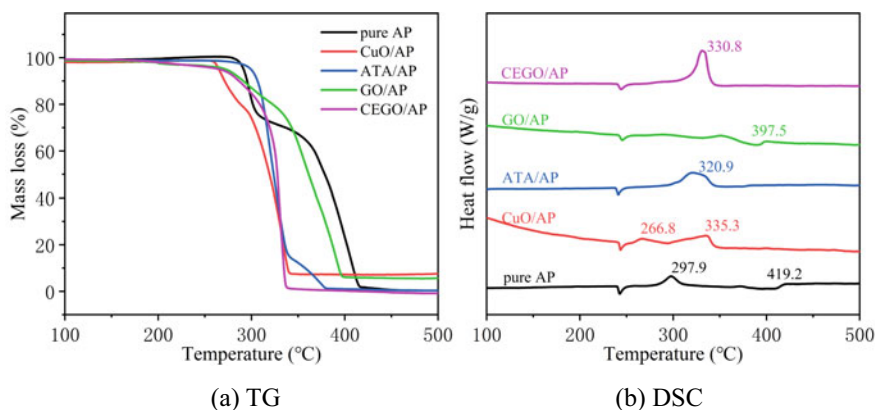


Fig. 4.2.7 TG (a) and DSC (b) curves of pure AP and AP composites at a heating rate of 10 °C/min

then affected the electron transport, thereby adversely affecting the catalytic effect of AP. In addition, the temperature decomposition peak of ATA/AP was 320.9 °C, which was slightly earlier than that of CEGO/AP, but the heat release (1042.0 J/g) was significantly lower than that of CEGO/AP, meant that the catalytic effect of ATA on AP was mainly due to energy content and preferential thermal decomposition, while CEGO was an excellent candidate combustion catalyst that could actually accelerate the thermal decomposition of AP.

To further study the pyrolysis of pure AP and AP composites, the thermal decomposition kinetic parameters were calculated. The DSC curves of pure AP and AP composites at different heating rates are shown in Fig. 4.2.8.

According to the T_H at different heating rates (Fig. 4.2.9), the figures were plotted with $1000/T_p$ and $\ln(\beta/T_p^2)$ as the abscissa and ordinate, respectively, by linear fitting, and the corresponding $\ln(\beta/T_p^2) \sim 1000/T_p$ diagram of pure AP and AP composites are shown in Fig. 4.2.9.

The Kissinger method was employed to calculate the thermal decomposition kinetic parameters of the pure AP and AP composites; the corresponding equation of this method can be expressed as follows:

$$\ln\left(\frac{\beta}{T_p^2}\right) = -\frac{E_a}{RT_p} + \ln\left(\frac{AR}{E_a}\right) \quad (42.1)$$

where β denotes the heating rate (K/min), E_a denotes the activation energy (kJ/mol), A denotes the pre-exponential factor (min^{-1}), and R represents the molar gas constant ($8.314 \text{ J mol}^{-1} \text{ K}^{-1}$). Further, E_a and A of pure AP and AP composites can be obtained according to the linear fitting equations in Fig. 4.2.9; the results are summarised in Table 4.2.2.

$$T_{p0} = T_{pi} - a\beta_i - b\beta_i^2 - c\beta_i^3 \quad (42.2)$$

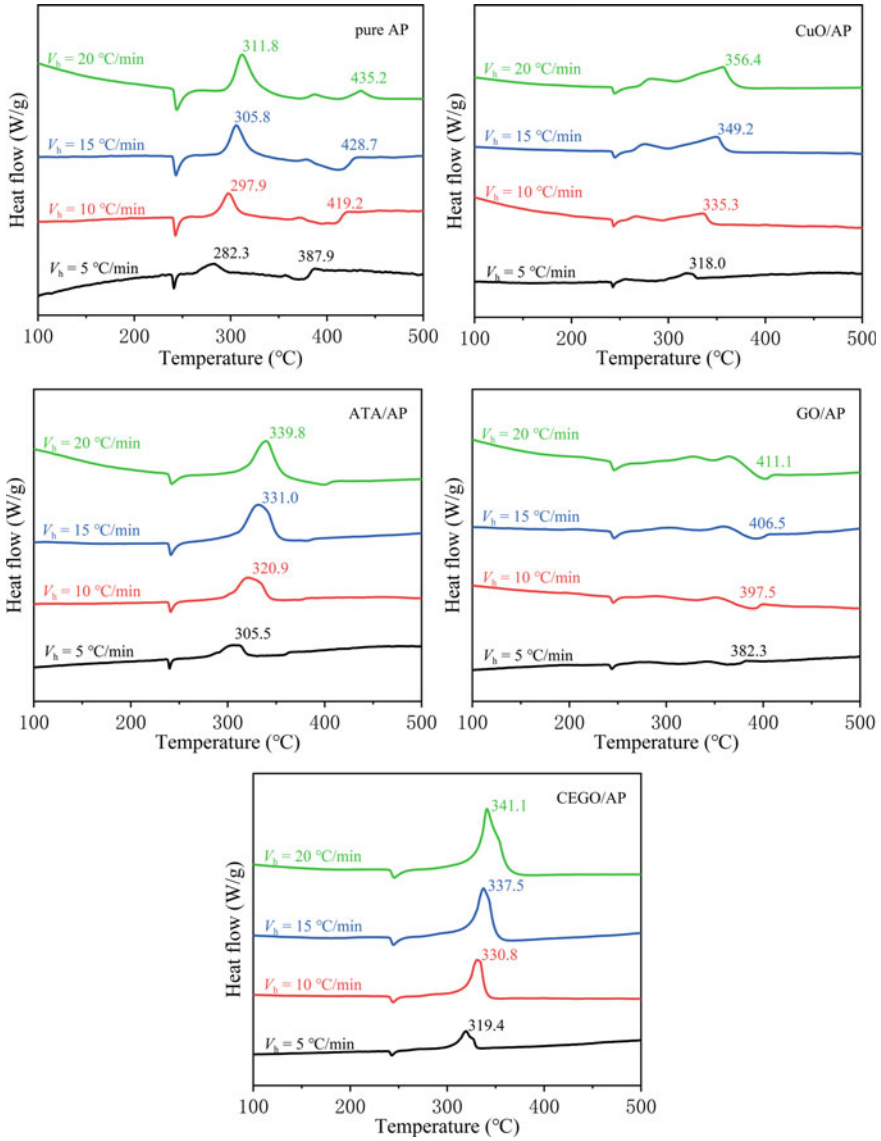


Fig. 42.8 DSC curves of pure AP and AP composites at different heating rates

$$\Delta S^\ddagger = R \left[\ln A - \ln \frac{k_B T_{p0}}{h} \right] \quad (42.3)$$

$$\Delta H^\ddagger = E_a - RT_{p0} \quad (42.4)$$

Fig. 42.9 The $\ln(\beta/T_p^2)$ $\sim 1000/T_p$ diagram of pure AP and AP composites

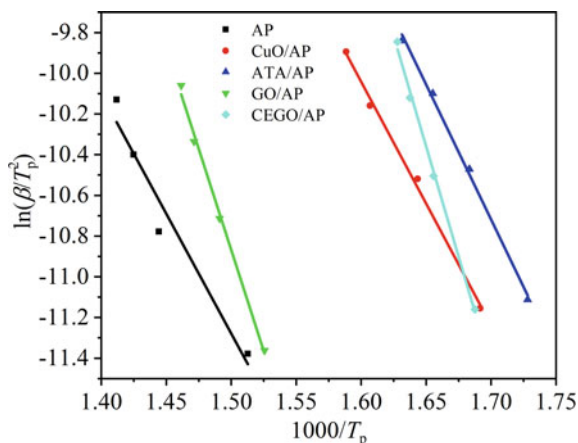


Table 42.2 Kinetics, thermodynamics and thermal stability parameters of pure AP and AP composites

| Sample | T_{p0} (°C) | $\ln A$ | E_a (kJ/mol) | ΔS^\ddagger (J mol ⁻¹ K ⁻¹) | ΔH^\ddagger (kJ/mol) | ΔG^\ddagger (kJ/mol) |
|---------|---------------|---------|----------------|--|------------------------------|------------------------------|
| AP | 316.0 | 15.8 | 97.9 | -153.6 | 93.0 | 183.5 |
| CuO/AP | 300.6 | 18.5 | 99.5 | -130.7 | 94.7 | 169.7 |
| ATA/AP | 280.8 | 21.3 | 110.2 | -106.9 | 105.6 | 164.8 |
| GO/AP | 359.1 | 28.8 | 164.9 | -45.9 | 159.7 | 188.7 |
| CEGO/AP | 301.7 | 35.4 | 180.2 | 9.7 | 175.4 | 169.8 |

$$\Delta G^\ddagger = \Delta H^\ddagger - T_{p0} \Delta S^\ddagger \quad (42.5)$$

where T_{pi} represents the decomposition peak temperature at a specific heating rate β_i , T_{p0} (K) is the corresponding decomposition peak temperature is when β approaches 0, k_B represents the Boltzmann constant (1.381×10^{-23} J/K), and h denotes the Planck constant (6.626×10^{-34} J s); ΔS^\ddagger , ΔH^\ddagger and ΔG^\ddagger are the activation entropy, enthalpy and Gibbs free energy, respectively.

To obtain ΔS^\ddagger , ΔH^\ddagger and ΔG^\ddagger of the decomposition reaction of pure AP and AP composites, the peak temperature (T_{p0}) should be calculated using Eq. (42.2). Then, Eqs. (42.3)–(42.5) can be used to calculate the relevant parameters in Table 42.2.

The ΔG^\ddagger of CEGO/AP was 169.8 kJ/mol, which was 13.7 kJ/mol lower than that of pure AP, and the corresponding T_{p0} significantly advanced. It is indicated that CEGO has a significant catalytic effect on pure AP. Moreover, compared with pure AP and other AP composites, the ΔS^\ddagger of CEGO/AP was the largest and positive, indicating that the confusion degree of CEGO/AP was high, which meant that CEGO could facilitate the thermal decomposition reaction of AP.

42.4 Conclusion

In summary, using the co-ordination modification method, a new energetic combustion catalyst CEGO was successfully synthesised. Then, DSC and TG were used to study the catalytic performance of CEGO/AP and other AP composites, and the corresponding kinetic and thermodynamic parameters were analysed. The results showed that CEGO had a significant catalytic effect on the thermal decomposition of AP, and the heat release of AP considerably increased after adding 5-wt% CEGO. Overall, these results show that the synthesis of CEGO by co-ordination modification paves a pathway for developing energetic combustion catalysts.

Acknowledgements This work was financially supported by the National Natural Science Foundation of China (Project No. 21805139, 22005144 and 22005145), Natural Science Foundation of Jiangsu Province (BK20200471) and the Fundamental Research Funds for the Central Universities (No. 30920041106, 30921011203).

Notes The authors declare no competing financial interest.

References

1. S. Chaturvedi, P.N. Dave, A review on the use of nanometals as catalysts for the thermal decomposition of ammonium perchlorate. *J. Saudi Chem. Soc.* **17**(2), 135–149 (2013)
2. S.G. Hosseini, M.A. Alavi, A. Ghavi et al., Modeling of burning rate equation of ammonium perchlorate particles over Cu-Cr-O nanocomposites. *J. Therm. Anal. Calorim.* **119**(1), 99–109 (2015)
3. J. Yang, W. Zhang, Q. Liu et al., Porous ZnO and ZnO-NiO composite nano/microspheres: synthesis, catalytic and biosensor properties. *RSC Adv.* **4**(93), 51098–51104 (2014)
4. Q. Yan, F. Zhao, K.K. Kuo et al., Catalytic effects of nano additives on decomposition and combustion of RDX-, HMX-, and AP-based energetic compositions. *Prog. Energy Combust. Sci.* **57**, 75–136 (2016)
5. N. Yan, L. Qin, J. Li et al., Atomic layer deposition of iron oxide on reduced graphene oxide and its catalytic activity in the thermal decomposition of ammonium perchlorate. *Appl. Surf. Sci.* **451**, 155–161 (2018)
6. G. Hao, H. Li, C. Mao et al., Preparation of nano-Cu-Fe composite metal oxides via a mechanical grinding method and its catalytic performance for the thermal decomposition of ammonium perchlorate. *Combust. Sci. Technol.* **193**(6), 1–18 (2019)
7. G. Singh, I. Kapoor, R. Dubey et al., Preparation, characterization and catalytic behavior of CdFe₂O₄ and Cd nanocrystals on AP, HTPB and composite solid propellants, Part: 79. *Thermochim. Acta* **511**(1–2), 112–118 (2010)
8. M.A. Fertassi, K.T. Alali, Q. Liu et al., Catalytic effect of CuO nanoplates, a graphene (G)/CuO nanocomposite and an Al/G/CuO composite on the thermal decomposition of ammonium perchlorate. *RSC Adv.* **6**(78), 74155–74161 (2016)
9. Y. Yuan, W. Jiang, Y. Wang et al., Hydrothermal preparation of Fe₂O₃/graphene nanocomposite and its enhanced catalytic activity on the thermal decomposition of ammonium perchlorate. *Appl. Surf. Sci.* **303**, 354–359 (2014)
10. D. Zhang, Q. Li, R. Li et al., Significantly enhanced thermal decomposition of mechanically activated ammonium perchlorate coupling with nano copper chromite. *ACS Omega* **6**(24), 16110–16118 (2021)

11. E. Alizadeh-Gheshlaghi, B. Shaabani, A. Khodayari et al., Investigation of the catalytic activity of nano-sized CuO, Co₃O₄ and CuCo₂O₄ powders on thermal decomposition of ammonium perchlorate. *Powder Technol.* **217**, 330–339 (2012)
12. A.C. Neto, F. Guinea, N. Peres et al., The electronic properties of graphene. *Rev. Mod. Phys.* **81**(1), 109–162 (2009)
13. S. Stankovich, D.A. Dikin, G. Dommett et al., Graphene-based composite materials. *Nature* **442**(7100), 282–286 (2006)
14. Y. Zhu, S. Murali, W. Cai et al., Graphene and graphene oxide: synthesis, properties, and applications. *ChemInform* **22**(35), 3906–3924 (2010)
15. A.A. Balandin, S. Ghosh, W. Bao et al., Superior thermal conductivity of single-layer graphene. *Nano Lett.* **8**(3), 902–907 (2008)
16. N. Li, Z. Geng, M. Cao et al., Well-dispersed ultrafine Mn₃O₄ nanoparticles on graphene as a promising catalyst for the thermal decomposition of ammonium perchlorate. *Carbon* **54**, 124–132 (2013)
17. J. Zhu, G. Zeng, F. Nie et al., Decorating graphene oxide with CuO nanoparticles in a water-isopropanol system. *Nanoscale* **2**(6), 988–994 (2010)
18. T. Kuila, S. Bose, A.K. Mishra et al., Chemical functionalization of graphene and its applications. *Prog. Mater. Sci.* **57**(7), 1061–1105 (2012)
19. S. Niyogi, E. Bekyarova, M.E. Itkis et al., Solution properties of graphite and graphene. *J. Am. Chem. Soc.* **128**(24), 7720–7721 (2006)
20. J. Azevedo, L. Fillaud, C. Bourdillon et al., Localized reduction of graphene oxide by electro-generated naphthalene radical anions and subsequent diazonium electrografting. *J. Am. Chem. Soc.* **136**(13), 4833–4836 (2014)
21. W. Zhang, Q. Luo, X. Duan et al., Nitrated graphene oxide and its catalytic activity in thermal decomposition of ammonium perchlorate. *Mater. Res. Bull.* **50**, 73–78 (2014)
22. K. Pytlakowska, M. Pilch, B. Hachula et al., Energy dispersive X-ray fluorescence spectrometric determination of copper, zinc, lead and chromium species after preconcentration on graphene oxide chemically modified with mercapto-groups. *J. Anal. At. Spectrom.* **34**(7), 1416–1425 (2019)
23. L. Hostert, S.F. Blaskiewicz, J.E. Fonsaca et al., Imidazole-derived graphene nanocatalysts for organophosphate destruction: powder and thin film heterogeneous reactions. *J. Catal.* **356**, 75–84 (2017)
24. N.A. Kumar, H. Choi, Y.R. Shin et al., Polyaniline-grafted reduced graphene oxide for efficient electrochemical supercapacitors. *ACS Nano* **6**(2), 1715–1723 (2012)
25. Q. Yan, A. Cohen, N. Petrutik et al., Highly insensitive and thermostable energetic coordination nanomaterials based on functionalized graphene oxides. *J. Mater. Chem. A* **4**, 9941–9948 (2016)
26. A. Cohen, Y. Yang, Q. Yan et al., Highly thermostable and insensitive energetic hybrid coordination polymers based on graphene oxide-Cu(II) complex. *Chem. Mater.* **28**(17), 6118–6126 (2016)
27. Y. Liu, C. He, Y. Tang et al., Tetrazolyl and dinitromethyl groups with 1,2,3-triazole lead to polyazole energetic materials. *Dalton Trans.* **48**(10), 3237–3242 (2019)
28. C. Zheng, Q. Qian, Y. Liu et al., Synthesis, crystal structure and characterizations of new 3,4,7,8-tetrachloro-1,10-phenanthroline Zn(II) complex. *J. Chem. Crystallogr.* **40**(1), 19–24 (2010)
29. Z. Guo, X. Liu, X. Chen et al., Design and synthesis of two energetic coordination polymers based on copper ion and 1H,1'H-[5,5'-bitetrazole]-1,1'-diol: a comparative study of the structure-property relationships. *J. Solid State Chem.* **268**, 55–61 (2018)
30. Y. Wang, L. Yi, X. Yang et al., Synthesis, crystal structure, and characterization of new tetranuclear Ag(I) complexes with triazole bridges. *Inorg. Chem.* **45**(15), 5822–5829 (2006)
31. R.L. Blaine, H.E. Kissinger, Homer Kissinger and the Kissinger equation. *Thermochim. Acta* **540**, 1–6 (2012)